Compositional Analysis of ssDNA-coated Single-Wall Carbon Nanotubes through UV Absorption Spectroscopy

Ali A. Alizadehmojarad,[†] Sergei M. Bachilo,[†] and R. Bruce Weisman*[,†,‡]

[†] Department of Chemistry and the Smalley-Curl Institute, Rice University, Houston, TX 77005 United States

[‡] Department of Materials Science and NanoEngineering, Rice University, Houston, TX 77005 United States

Abstract

Aqueous suspensions of single-wall carbon nanotubes (SWCNTs) coated by ssDNA are analyzed using UV absorption and total carbon measurements. The results give absolute average concentrations of both components in samples without free ssDNA. From those values, the average mid-UV SWCNT absorptivity is deduced for three different batches of relatively small diameter nanotubes: two HiPco and one CoMoCAT. The absorptivity values enable the use of simple spectrophotometry to measure absolute concentrations of similar SWCNT samples in aqueous SDS. The results also quantify the mass ratio of ssDNA to SWCNT, defining the average number of nanotube carbon atoms suspended by one ssDNA strand of $T_{15}GT_{15}$ or $T_{30}G$. Comparing this experimental parameter with results from replica exchange molecular dynamics simulations of one ssDNA strand freely adsorbed on a (6,5) segment shows close agreement between the computed number of SWCNT atoms covered per strand and the measured number of SWCNT atoms suspended per strand.

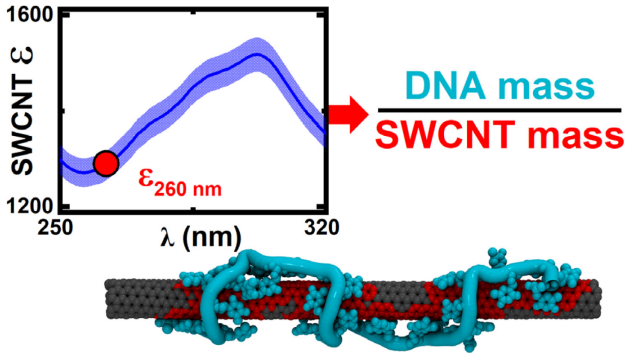

Keywords: replica exchange molecular dynamics; SWCNT extinction coefficients; UV absorptivity

Single-wall carbon nanotubes (SWCNTs) are a widely studied family of artificial nanomaterials with unusual physical and chemical properties and many potential applications. As-produced SWCNT samples contain a variety of distinct and well-defined structural forms, each designated by a pair of integers, (*n*,*m*).[1] A variety of scientific and engineering applications, including sorting SWCNTs by structure, require raw samples to be disaggregated and dispersed into stable liquid suspensions with SWCNT surfaces coated by surfactants or polymers. Short strands of single-stranded DNA (ssDNA) have emerged as one of the most important coating types.[2–8]

In working with any suspension or solution, it is usually necessary to know the concentration of solute. This key parameter is not simple to determine for most SWCNT samples, partly because of their inhomogeneous compositions. Optical absorption measurements are quick, inexpensive, and non-destructive, but require knowledge of absolute absorptivity values. These (*n*,*m*)-specific values are available for the near-infrared (E_{11}) transitions of a number of semiconducting (*n*,*m*) species.[9–11] However, the use of those values to find total SWCNT concentrations is hampered by the need to deconvolute congested near-infrared absorption spectra,[12] the incomplete set of known semiconducting absorptivities, and the difficulty of accounting for metallic SWCNTs. Previous studies of larger diameter SWCNTs grown by arc discharge have measured their broad optical absorptions at selected visible or near-infrared wavelengths and deduced absorptivities corresponding to total SWCNT content.[13–16]

UV spectroscopy may offer a more promising spectral region for estimating total SWCNT concentrations because all (*n*,*m*) species show strong absorptions in this range. The broader overlapped peaks from different species blur the spectral structure and make it simpler to deduce the total sample concentration from measurements at single wavelengths. A potential complication in this approach is subtracting the interfering absorption from the agent used to suspend the nanotubes,[17] but such spectral interference is absent for samples suspended in SDS, a common surfactant that is transparent in the mid-UV.

Here we report a method to measure overall UV extinction coefficients for samples of relatively small diameter SWCNTs grown by different methods. In our approach, illustrated in the flow chart of Figure 1, we prepare stable SWCNT dispersions in specific ssDNA oligos and then remove free

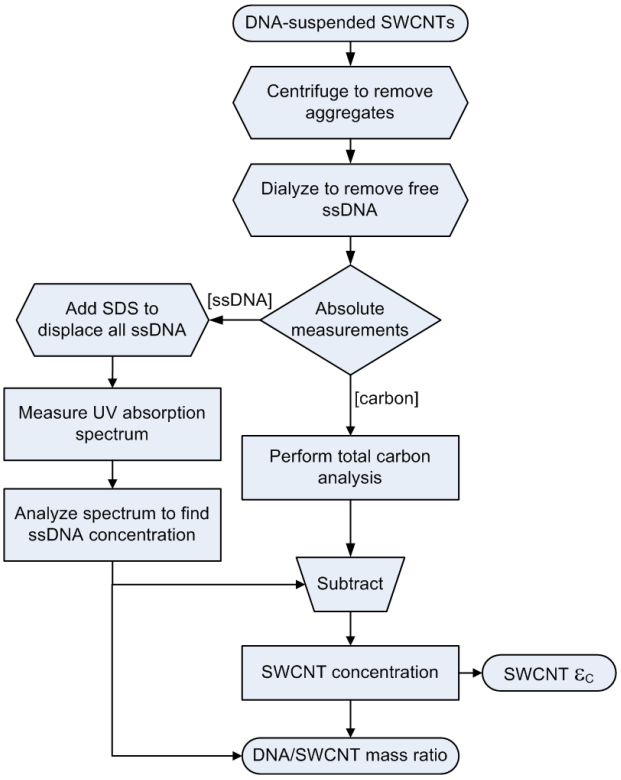

Figure 1. Flowchart illustration of the method for determining ssDNA and SWCNT concentrations, SWCNT UV molar absorptivity, and the DNA/SWCNT mass ratio in samples of SWCNTs dispersed in ssDNA.

ssDNA by dialysis. The entire carbon concentration (from ssDNA and SWCNTs) in a dialyzed sample is measured with a total carbon analyzer. We separately measure the ssDNA concentration by UV absorption spectroscopy after adding SDS to displace ssDNA from the SWCNT surface and give unperturbed ssDNA spectra. Using the quantitative concentrations of ssDNA and total carbon, we compute the absolute SWCNT concentration by difference and then find SWCNT extinction coefficients in the UV spectral region. The resulting values enable a simple spectrophotometric assay of SWCNT concentration that should be useful in many applications. In addition, our sample analyses also quantify the mass ratios of surface-adsorbed ssDNA to SWCNTs, revealing the average nanotube length coated by one ssDNA strand. This parameter provides a needed experimental check on computational simulations of ssDNA structures on SWCNTs. We have applied this check to Replica Exchange Molecular Dynamics (REMD) simulations by comparing their predicted coverages with measured values. The results generally

validate the simulations and increase confidence in their insights into the structures of ssDNA oligos coating SWCNTs.

To prepare our samples, we purchased custom-synthesized DNA oligonucleotides from Integrated DNA Technologies, Inc. and dissolved them in a solution of 0.1 M sodium chloride and 0.06 M sodium phosphate buffer (pH=7.4). We used SWCNTs produced from HiPco and CoMoCAT growth processes (Rice reactor batches 195.1 and 189.1, and Sigma-Aldrich product #773735, respectively). The DNA to SWCNT mass ratio at the beginning of sample preparation was kept at 2:1 for all samples. The mixtures were tip sonicated at 6 W power (3 mm tip, Branson digital sonifier) for 20 active minutes (50% duty cycle with 60 s cycle length). The suspended SWCNT mixtures were centrifuged twice for 90 minutes at 13000g in a Biofuge-13 (Baxter Scientific), with the top 80 percent of supernatant extracted each time. For characterization, a stock solution was prepared by diluting the final supernatant with the phosphate buffer described above.

Our DNA-dispersed SWCNT samples initially contained both free and SWCNT-bound DNA. To selectively analyze for the DNA adsorbed onto nanotubes, it was necessary to remove the free DNA. We achieved this through sample dialysis using 10 mL Spectra/Por Float-A-Lyzer G2 devices with a molecular weight cutoff of 100 kDa. This dialysis cutoff was chosen to retain SWCNTs while passing free DNA oligos. We carefully dialyzed samples twice for 24 h, with ~6 mL of the stock solution in the dialysis tube immersed in ~480 mL of the phosphate buffer solution. Further dialysis led to some sample loss but did not change the ratio of DNA to SWCNT concentrations, indicating efficient removal of free DNA. Absorption and fluorescence spectra of the sample before and after dialysis showed that the SWCNT near-IR fluorescence remained almost unchanged, while UV absorption in the DNA absorption region dropped significantly (see Figure S1). This observation confirmed the successful removal of free DNA and non-emissive carbonaceous impurities that contribute to background absorption.

SDS surfactant was then used to displace bound DNAs from the SWCNT surface. We dissolved solid SDS into the dialyzed samples to reach 1% (w/v) SDS concentration in the dispersion. The sample with SDS was first bath sonicated for 20 minutes to facilitate coating displacement. However, visible-NIR absorption and fluorescence spectra following this step showed peak positions and shapes indicating incomplete coating displacement. We therefore applied further agitation through tip sonication for 2 min at 6 W power (3 mm tip, Branson digital

sonifier). After this, fluorescence peak positions matched those of samples dispersed directly in SDS, indicating successful displacement of the original DNA coating.

Our sample characterization involved visible and near-infrared (NIR) absorption spectra measured with a prototype model NS2 NanoSpectralyzer (Applied Nano-Fluorescence, LLC). The same instrument was used to capture fluorescence spectra at fixed excitation wavelengths (642, 659 and 784 nm). We measured UV-vis absorption spectra with a Cary 60 spectrophotometer (Agilent). The optical path length for all measurements was 1 cm. Total organic carbon (TOC) analyses of dialyzed samples were performed with a model TOC-V_{CPN} (Shimadzu). In each TOC analysis, 75 µL of sample was sparged for 2 minutes to remove dissolved CO_2 before injection into the combustion tube containing a catalyst designed for high detection sensitivity.

We performed atomistic molecular dynamics (MD) simulations to study structures of $T_{15}GT_{15}$ and $T_{30}G$ ssDNA oligos adsorbed on (6,5) SWCNTs. VMD software was used to build MD simulation systems and visualize results.[18] The Solvate and Ionize VMD plugins were used for solvating and neutralizing ssDNA-SWCNT hybrids with the TIP3P water model and 0.1 M NaCl content, respectively. We ran MD simulations with the NAMD 2.13 package,[19] using the CHARMM36 force fields to describe all species.[20,21] To match experimental conditions, a temperature of 300 K and a pressure of 1 bar were maintained in an NPT ensemble via Langevin dynamics with a Langevin constant of γ_{Lang}= 1.0 ps^{-1}. For simulations we applied periodic boundary conditions in all directions, and the Particle Mesh Ewald (PME) method was used for evaluating long-range Coulomb interaction energies.[22] An integration time step of 2.0 fs was set for simulations. We used 1000 steps of energy minimization followed by 2 ns of equilibration simulations before performing replica exchange MD (REMD) runs. During the preparation stage, the ssDNA-SWCNT hybrid was constrained with a harmonic force constant of 1 kcal/(mol $Å^2$). For the subsequent production MD run, we modeled a single ssDNA strand wrapping around a (6,5) SWCNT, with at least 16,000 atoms in a 3.6 × 3.6 × 12.0 nm^3 box.

The REMD simulations were employed for more extensive study of ssDNA conformations. Our previous research has shown that REMD is a robust method to explore many different ssDNA conformations on different SWCNT chiralities.[23–25] Here, a (6,5) SWCNT wrapped with a single ssDNA strand was solvated and neutralized with water molecules and 0.1 M sodium chloride. We applied periodic boundary conditions in three dimensions with the SWCNT ends meeting their

periodic images. Energy minimization and 100 ps NVT simulations were run to heat the systems to room temperature before production runs. We implemented REMD simulations in an NVT ensemble with an exchange time of 2.0 ps and average exchange ratio of 25%. There were 80 replicas covering a temperature range of 290 to 727 K. We used a time step of 2 fs and saved trajectories every 2 ps. Replicas were run in parallel up to 160 ns, giving a total simulation time of 80×160 ns = 12.8 μs. For every replica, 80,000 snapshots were collected, of which only the last 40,000 (from the last 80 ns) of room temperature replicas were analyzed as consistent with experimental conditions. To compute the number of SWCNT carbon atoms covered by the adsorbed DNA, we found the distance between each SWCNT atom and the nearest DNA atom. Those within a cutoff distance were counted as covered. Figure S2 shows the distribution function of those distances and illustrates the 0.425 to 0.518 nm range taken as plausible cutoffs for defining coverage. We chose 0.471 nm, a central value within this range, as the cutoff distance to calculate the numbers of SWCNT atoms covered. Another extracted quantity was the DNA strand end-to-end distance, measured along the nanotube axis between centers of mass of the two most widely separated nucleobases. The coverage and end-to-end distance were computed for each REMD snapshot.

To experimentally determine UV absorptivities, we dispersed SWCNTs using the ssDNA sequences $T_{15}GT_{15}$ and $T_{30}G$, which were taken to represent medium length oligos and are more easily displaced than similar guanine-rich sequences. The resulting suspensions were stable and showed well-resolved near-IR absorption and fluorescence spectra (see Figure 2 and Figure S1). Unsorted SWCNTs from three sources were studied: one grown by the CoMoCAT method and two batches grown by the HiPco process. Figures 2a and 2d and Figures S3a and S3b show the fluorescence and absorption spectra of these different SWCNT batches dispersed in $T_{15}GT_{15}$, before and after DNA had been displaced by SDS. Figures S4a to S4f show the comparable spectra dispersed in $T_{30}G$. These figures also clearly illustrate the expected blue shifts, particularly for E_{11} transitions, caused by the addition of SDS to displace adsorbed ssDNA. Such displacement of ssDNA by SDS and other surfactants has been documented previously.[26–28]

Figure 3a shows the separate UV-Vis absorption spectra of $T_{15}GT_{15}$ ssDNA and of one of our HiPco samples dispersed in SDS, which is transparent in this spectral range. In Figures 3b to 3d,

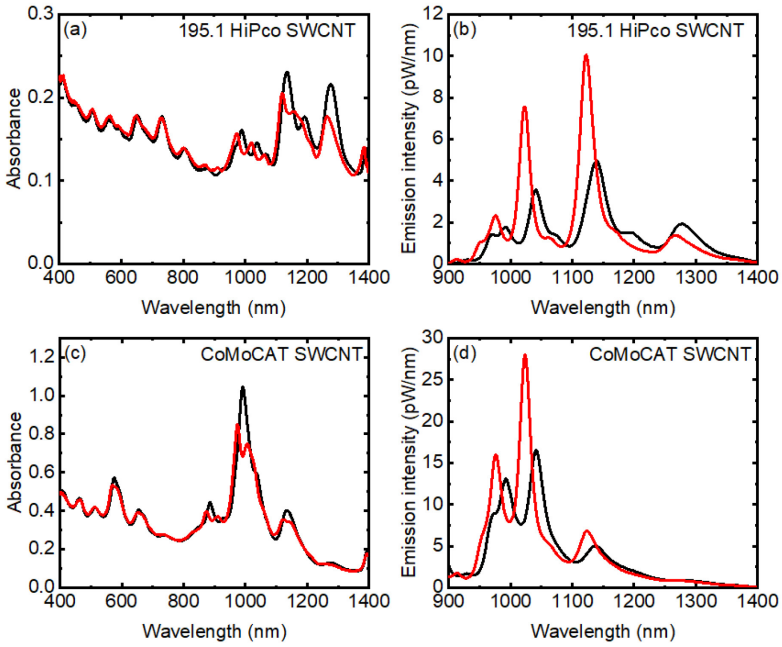

Figure 2. (a) Absorption and (b) Fluorescence spectra of 195.1 HiPco SWCNTs dispersed in $T_{15}GT_{15}$. (c) Absorption and (d) Fluorescence spectra of CoMoCAT SWCNTs dispersed in $T_{15}GT_{15}$. Curves show the spectra before (black) and after (red) DNA displacement by SDS.

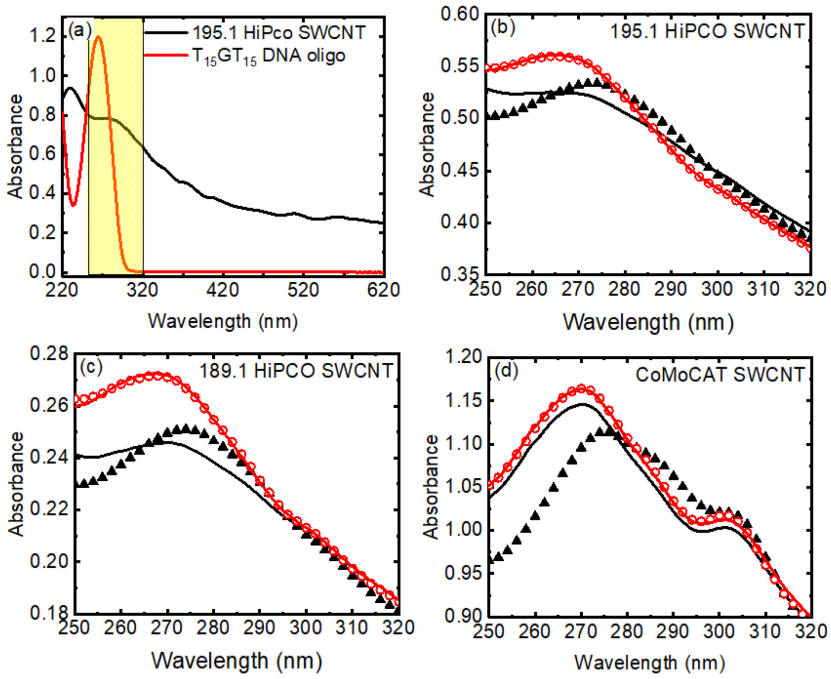

Figure 3. (a) UV absorption spectra of aqueous $T_{15}GT_{15}$ DNA (red curve) and 195.1 HiPco SWCNTs dispersed in SDS (black curve). Linear combinations of these two spectra were used to fit experimental data in the three other frames of this figure. Symbols in (b), (c), and (d) show absorption spectra of 195.1 HiPco SWCNTs in $T_{15}GT_{15}$, CoMoCAT SWCNTs in $T_{15}GT_{15}$, and 189.1 HiPco SWCNTs in $T_{15}GT_{15}$, respectively. The solid black triangles and red open circles were measured before and after DNA displacement by SDS. Solid curves show computed best fits.

absorbance data for ssDNA dispersions of three SWCNT sources are plotted between 250 and 320

nm as black triangles. In this region, absorptions of the DNA bases overlap with SWCNT E_{33} and E_{44} transitions and π-plasmon bands, and the couplings between electronic transitions of SWCNTs and the ssDNA coatings are strong enough to perturb their peak positions and intensities. The spectra therefore cannot be well modeled as a linear combination of the spectra of aqueous ssDNA and SDS-suspended SWCNTs. This mismatch is illustrated by deviations of the measured data from the linear combination best fits (black curves). However, adding SDS caused the ssDNA to desorb, removing the couplings and giving the measured data shown as red circles. These could be accurately fit as superpositions of spectra of free ssDNA and SWCNTs in SDS (the red curves). Similar spectra and fits for the second ssDNA oligo are plotted in Figure S5. Because the absolute UV absorptivity spectra of ssDNA oligos are well known, this spectral fitting gave us absolute ssDNA concentrations and therefore the masses of oligos that had been adsorbed to SWCNTs in our dialyzed samples.

Table 1. Quantitative analyses of three types of SWCNT samples dispersed in $T_{15}GT_{15}$ and $T_{30}G$ ssDNA.

Quantity	195.1 HiPco		189.1 HiPco		CoMoCAT	
	$T_{15}GT_{15}$	$T_{30}G$	$T_{15}GT_{15}$	$T_{30}G$	$T_{15}GT_{15}$	$T_{30}G$
Mean SWCNT diam.[1] (nm)	0.885		0.840		0.799	
DNA conc.[2] (mg/L)	3.23 ± 0.08	3.33 ± 0.12	1.91 ± 0.05	3.16 ± 0.07	4.76 ± 0.17	5.43 ± 0.15
DNA carbon conc.[3] (mg/L)	1.29 ± 0.03	1.33 ± 0.05	0.76 ± 0.02	1.26 ± 0.03	1.90 ± 0.07	2.16 ± 0.06
Total carbon conc. [4] (mg/L)	4.68 ± 0.03	4.44 ± 0.10	2.26 ± 0.14	3.36 ± 0.10	5.53 ± 0.06	7.21 ± 0.13
SWCNT carbon conc.[5] (mg/L)	3.39 ± 0.05	3.12 ± 0.11	1.50 ± 0.14	2.10 ± 0.10	3.63 ± 0.09	5.04 ± 0.14
DNA / SWCNT mass ratio	0.95 ± 0.03	1.07 ± 0.06	1.28 ± 0.13	1.50 ± 0.08	1.31 ± 0.06	1.08 ± 0.04
SWCNT ε_{260} (M_C^{-1} cm^{-1}) [6]	1660 ± 24	1800 ± 66	1760 ± 172	1920 ± 94	1350 ± 60	1200 ± 36

[1] Estimated from analysis of fluorescence spectra
[2] Computed from UV absorption
[3] Total carbon content from UV absorption and stoichiometry
[4] Measured directly with a total carbon analyzer
[5] Calculated by subtracting DNA carbon concentration from total carbon concentration
[6] Based on molar concentration of SWCNT carbon atoms

The second component from UV spectral fitting represents the product of SWCNT UV absorptivity times SWCNT concentration, averaged over the (*n*,*m*) distribution in the sample. To deduce the absorptivity, we therefore needed to find the nanotube concentration. Our method for this was to analyze the dialyzed ssDNA-SWCNT dispersions with a total organic carbon (TOC) instrument. This provided the sum of carbon contents from SWCNTs and their ssDNA coatings. It was simple to compute the contribution from carbon in ssDNA based on the known oligo composition and the absolute concentration result described above. Subtracting this from the total carbon content then gave the absolute SWCNT mass, which we divided into the second UV spectral fitting component to obtain the SWCNT absolute absorptivity spectrum. Table 1 lists the measured quantities in this analysis for suspensions of the three SWCNT sources in $T_{15}GT_{15}$ and in $T_{30}G$. The values listed are the averages of at least three replicate runs, with uncertainties shown as standard deviations found by error propagation. The deduced molar absorptivity spectra, expressed per mole of carbon atoms, are plotted in Figure 4 for the three SWCNT sources (see Figure S9 for absorption cross section plots and Table S1 for numerical values). Below 305 nm, the spectrum for CoMoCAT-grown SWCNTs differs significantly from the HiPco spectra, presumably because CoMoCAT is highly enriched in smaller diameter SWCNTs, which do not show higher order transitions in this range. The two HiPco batches are similar to each other but

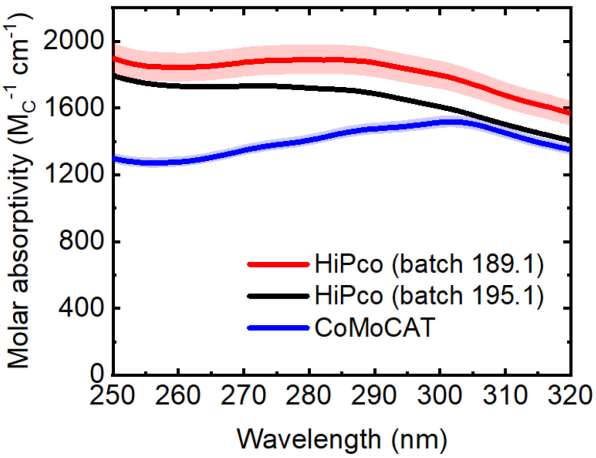

Figure 4. Deduced UV molar absorptivity spectra (based on carbon atom molar concentration) for CoMoCAT SWCNTs (blue curve) and HiPco batches 189.1 (red curve) and 195.1 (black curve). The shaded band around each curve shows estimated uncertainties based on replicate measurements.

show lower absorptivities for batch 195.1, which contains a slightly lower content of smaller diameter SWCNTs. (Sample average diameters were found from analysis of fluorescence spectra.[29]) Our average HiPco absorptivity at 273 nm is approximately 20% lower than the value reported by Attal et al.[17]

Table 2. Averaged experimental values for three different SWCNT batches of their DNA-to-SWCNT mass ratios, numbers of suspended SWCNT carbon atoms per DNA strand, SWCNT ε_{260} (based on carbon molar and mass concentrations), and absorption cross sections per carbon atom.

Quantity	195.1 HiPco	CoMoCAT	189.1 HiPco
DNA / SWCNT mass ratio	1.01 ± 0.03	1.19 ± 0.03	1.39 ± 0.07
# SWCNT C atoms / DNA strand	775 ± 23	658 ± 17	563 ± 28
ε_{260} (M_C^{-1} cm^{-1})	1731 ± 35	1275 ± 35	1842 ± 96
ε_{260} (L mg^{-1} cm^{-1})	0.144 ± 0.003	0.106 ± 0.003	0.154 ± 0.008
σ_{260} (10^{-18} cm^2 / C)	6.6 ± 0.13	4.9 ± 0.13	7.0 ± 0.37

Table 2 lists carbon molar absorptivities and mass absorptivities at 260 nm (ε_{260}), averaged over the two ssDNA coatings studied here. Using these values, any laboratory can perform quick and simple UV absorption spectroscopy to closely estimate the absolute SWCNT concentrations of HiPco or CoMoCAT suspensions in SDS. Table 2 also shows the corresponding absorption cross sections per carbon atom.

In addition to these spectroscopic results, we have also found the DNA-to-SWCNT mass ratios in the dialyzed samples. These values, which are listed in Table 1, reveal the average number of nanotube carbon atoms suspended by one strand of the ssDNA oligo. That information is valuable for interpreting molecular dynamics simulations of ssDNA-coated SWCNT structures.

To illustrate, we have performed replica exchange molecular dynamics (REMD) simulations of (6,5) SWCNTs coated by $T_{15}GT_{15}$ or $T_{30}G$ ssDNA and compared the results to the experimentally obtained numbers of SWCNT carbon atoms suspended per DNA strand. Figure 5a shows that these REMD simulations gave an average end-to-end DNA distance of 9.2 nm with a distribution width of 1 nm. In Figure 5b we plot the final distribution of number of SWCNT carbon atoms covered per DNA strand (found using the algorithm described in Methods) computed from sets of structural

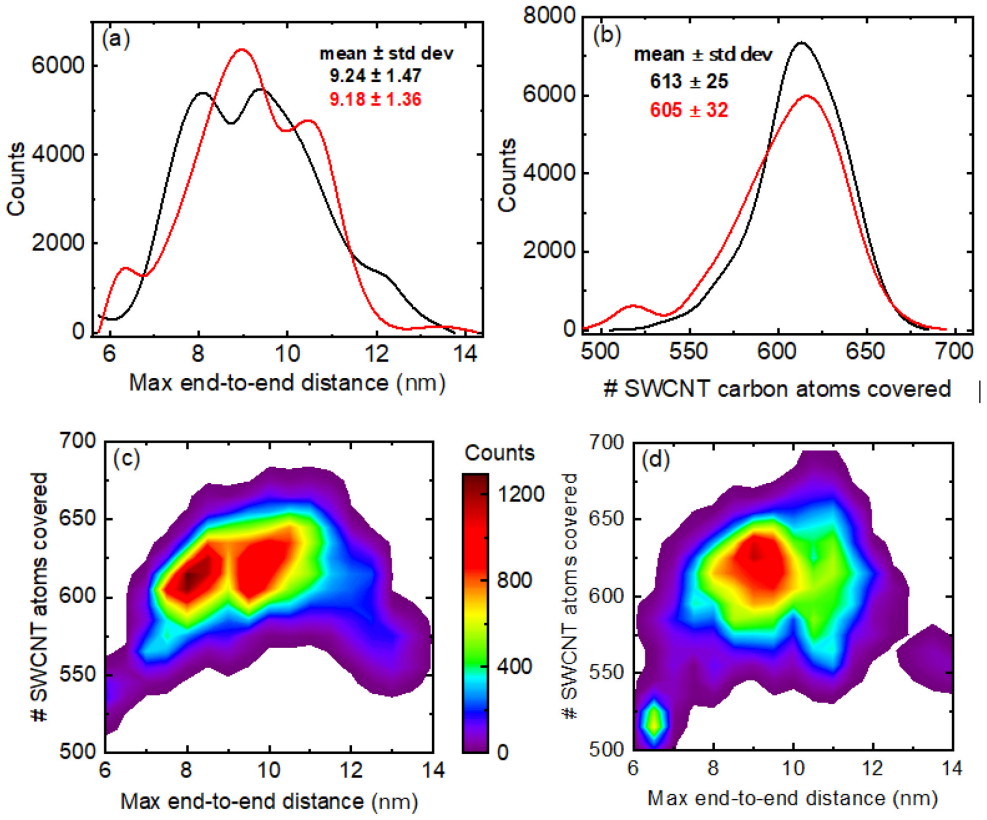

Figure 5. Results from REMD simulations of a 12 nm long (6,5) SWCNT coated by a single strand of $T_{15}GT_{15}$ (black curves) or $T_{30}G$ (red curves). (a) Distribution over snapshots of the maximum end-to-end distance of the DNA strand; (b) Distribution over snapshots of the number of SWCNT carbon atoms covered by a DNA strand; (c), (d) Frequency contour plots showing correlations between the number of covered SWCNT atoms and the maximum end-to-end distance for (c) $T_{15}GT_{15}$ or (d) $T_{30}G$.

snapshots for two separate REMD simulations of a single unhindered $T_{15}GT_{15}$ or $T_{30}G$ strand wrapping a 12 nm long (6,5) segment. The average value obtained from these two simulation sets was 609. REMD simulations have previously been used as a powerful method for exploring conformations of DNA oligos on SWCNTs.[24,25,29] However, none of the previous REMD simulation results were validated against experimental data. To avoid biasing the results, we started our simulations with structures corresponding to relatively high DNA-to-SWCNT mass ratios of ~1.44 before they were allowed to equilibrate.

Because surface coverage and axial length of adsorbed DNA are important quantities for understanding the structure of ssDNA-wrapped nanotubes, we examined the correlation between those values in our REMD simulations. The results are displayed as color-coded frequency contour plots in Figures 5c and 5d for the two oligos studied here. The absence of a significant diagonal

component in these plots shows that variations in DNA axial length are not correlated with variations in the number of covered SWCNT atoms. The physical basis for this finding can be seen from the structural snapshot in Figure S10, in which changes in the DNA wrapping pitch alter the locations but not the number of the yellow-colored covered SWCNT atoms that are adjacent to nucleobase atoms.

The REMD result for the number of covered SWCNT atoms per DNA strand is within 8% of the experimental value of 658 ± 17 (see Table 2) for the average number of suspended SWCNT atoms per DNA strand in the CoMoCAT sample (which has the highest (6,5) abundance). Although a typical snapshot (see Figure S10) illustrates that ~33% of the SWCNT atoms within the average DNA axial length of a DNA strand remain uncovered, the computation modeled only a single DNA strand. It therefore could not simulate interactions among strands that would lead to higher surface coverage, such as axial DNA compression[2] or overlapped helical wrapping motifs that cover exposed regions. More extensive computations that include a range of (*n*,*m*) species may clarify the role of such effects in this and similar systems. Our study shows that even though classical force fields lack precise descriptions of π-π stacking interactions between DNA bases and SWCNTs, MD simulations can still provide useful comparisons with experimental data for this important class of nanohybrids.

In summary, we have used a combination of UV absorption spectroscopy and total organic carbon measurements to quantify the composition of SWCNTs dispersed in ssDNA oligos. The analyses provide absolute UV extinction coefficients for three different SWCNT HiPco and CoMoCAT sample batches (averaged over their (*n*,*m*) distributions). These values are directly useful for finding absolute SWCNT concentrations in aqueous SDS suspensions through simple UV absorption measurements. In addition, our assays give the relative masses of ssDNA and SWCNTs in samples processed to remove free ssDNA. The experimental ratios reveal the average number of nanotube carbon atoms suspended per ssDNA strand, allowing comparison with modeling by replica exchange molecular dynamics calculations, which show a similar number of covered nanotube atoms per ssDNA strand. This study provides the first experimentally linked application of molecular dynamics for describing a key structural parameter in SWCNT-ssDNA interactions.

ASSOCIATED CONTENT

Supporting Information. Absorption and emission spectra illustrating dialysis purification; surface coverage plots from REMD simulations; spectra related to coating displacement and UV spectral fitting; deduced UV absorption cross section spectra for three SWCNT sample types; REMD structural snapshot for $T_{15}GT_{15}$ on a (6,5) SWCNT segment. This material is available free of charge via the Internet at http://pubs.acs.org.

AUTHOR INFORMATION

Corresponding Author

* E-mail: weisman@rice.edu.

ORCID

Ali A. Alizadehmojarad: 0000-0001-6806-5415

Sergei M. Bachilo: 0000-0001-5236-1383

R. Bruce Weisman: 0000-0001-8546-9980

Notes

The authors declare the following competing financial interest: R. B. W. has a financial interest in Applied NanoFluorescence, LLC, which manufactures some of the instruments used in this project.

ACKNOWLEDGMENTS

This research was supported by grants from the National Science Foundation (CHE-1803066 and CHE- 2203309). We thank Qilin Li for generously providing access to a TOC instrument.

References

(1) Reich, S.; Thomsen, C.; Maultzsch, J. *Carbon Nanotubes: Basic Concepts and Physical Properties*; John Wiley & Sons: Hoboken, 2008.

(2) Zheng, Y.; Alizadehmojarad, A. A.; Bachilo, S. M.; Weisman, R. B. Guanine-Specific Chemical Reaction Reveals SsDNA Interactions on Carbon Nanotube Surfaces. *Journal of Physical Chemistry Letters* **2022**, *13* (9), 2231–2236. https://doi.org/10.1021/acs.jpclett.2c00030.

(3) Sun, W.; Shen, J.; Zhao, Z.; Arellano, N.; Rettner, C.; Tang, J.; Cao, T.; Zhou, Z.; Ta, T.; Streit, J. K.; Fagan, J. A.; Schaus, T.; Zheng, M.; Han, S.-J.; Shih, W. M.; Maune, H. T.; Yin, P. Precise Pitch-Scaling of Carbon Nanotube Arrays within Three-Dimensional DNA Nanotrenches. *Science* **2020**, *368* (6493), 874–877. https://doi.org/10.1126/science.aaz7440.

(4) Zheng, Y.; Kim, Y.; Jones, A. C.; Olinger, G.; Bittner, E. R.; Bachilo, S. M.; Doorn, S. K.; Weisman, R. B.; Piryatinski, A.; Htoon, H. Quantum Light Emission from Coupled Defect States in DNA-Functionalized Carbon Nanotubes. *ACS Nano* **2021**, *15* (6), 10406–10414. https://doi.org/10.1021/acsnano.1c02709.

(5) Zheng, M.; Jagota, A.; Semke, E. D.; Diner, B. A.; McLean, R. S.; Lustig, S. R.; Richardson, R. E.; Tassi, N. G. DNA-Assisted Dispersion and Separation of Carbon Nanotubes. *Nat Mater* **2003**, *2* (5), 338–342. https://doi.org/10.1038/nmat877.

(6) Huang, X.; McLean, R. S.; Zheng, M. High-Resolution Length Sorting and Purification of DNA-Wrapped Carbon Nanotubes by Size-Exclusion Chromatography. *Analytical Chemistry* **2005**, *77* (19), 6225–6228. https://doi.org/10.1021/ac0508954.

(7) Zheng, Y.; Bachilo, S. M.; Weisman, R. B. Controlled Patterning of Carbon Nanotube Energy Levels by Covalent DNA Functionalization. *ACS Nano* **2019**, *13*, 8222–8228. https://doi.org/10.1021/acsnano.9b03488.

(8) Williams, R. M.; Lee, C.; Heller, D. A. A Fluorescent Carbon Nanotube Sensor Detects the Metastatic Prostate Cancer Biomarker UPA. *ACS Sensors* **2018**, *3* (9), 1838–1845. https://doi.org/10.1021/acssensors.8b00631.

(9) Streit, J. K.; Bachilo, S. M.; Ghosh, S.; Lin, C.-W.; Weisman, R. B. Directly Measured Optical Absorption Cross Sections for Structure-Selected Single-Walled Carbon Nanotubes. *Nano Letters* **2014**, *14* (3), 1530–1536. https://doi.org/10.1021/nl404791y.

(10) Sanchez, S. R.; Bachilo, S. M.; Kadria-Vili, Y.; Lin, C.-W.; Weisman, R. B. (N,m)-Specific Absorption Cross Sections of Single-Walled Carbon Nanotubes Measured by Variance Spectroscopy. *Nano Letters* **2016**, *16*, 6903–6909. https://doi.org/10.1021/acs.nanolett.6b02819.

(11) Schöppler, F.; Mann, C.; Hain, T. C.; Neubauer, F. M.; Privitera, G.; Bonaccorso, F.; Chu, D.; Ferrari, A. C.; Hertel, T. Molar Extinction Coefficient of Single Walled Carbon Nanotubes. *Journal of Physical Chemistry C* **2011**, *115*, 14682–14686.

(12) Naumov, A. V.; Ghosh, S.; Tsyboulski, D. A.; Bachilo, S. M.; Weisman, R. B. Analyzing Absorption Backgrounds in Single-Walled Carbon Nanotube Spectra. *ACS Nano* **2011**, *5*, 1639–1648.

(13) Ansón-Casaos, A.; González-Domínguez, J. M.; Lafragüeta, I.; Carrodeguas, J. A.; Martínez, M. T. Optical Absorption Response of Chemically Modified Single-Walled Carbon Nanotubes upon Ultracentrifugation in Various Dispersants. *Carbon* **2014**, *66*, 105–118. https://doi.org/10.1016/j.carbon.2013.08.048.

(14) Jeong, S. H.; Kim, K. K.; Jeong, S. J.; An, K. H.; Lee, S. H.; Lee, Y. H. Optical Absorption Spectroscopy for Determining Carbon Nanotube Concentration in Solution. *Synthetic Metals* **2007**, *157* (13–15), 570–574. https://doi.org/10.1016/j.synthmet.2007.06.012.
(15) Moore, V. C. Single Walled Carbon Nanotubes: Suspension in Aqueous/Surfactant Media and Chirality Controlled Synthesis on Surfaces. Ph.D. Thesis, Rice University, 2005, Vol. Ph.D.
(16) Zhao, B.; Itkis, M. E.; Niyogi, S.; Hu, H.; Zhang, J.; Haddon, R. C. Study of the Extinction Coefficients of Single-Walled Carbon Nanotubes and Related Carbon Materials. *Journal of Physical Chemistry B* **2004**, *108* (24), 8136–8141. https://doi.org/10.1021/jp037402o.
(17) Attal, S.; Thiruvengadathan, R.; Regev, O. Determination of the Concentration of Single-Walled Carbon Nanotubes in Aqueous Dispersions Using UV−Visible Absorption Spectroscopy. *Analytical Chemistry* **2006**, *78* (23), 8098–8104. https://doi.org/10.1021/ac060990s.
(18) Humphrey, W.; Dalke, A.; Schulten, K. VMD: Visual Molecular Dynamics. *Journal of Molecular Graphics* **1996**, *14* (1), 33–38. https://doi.org/10.1016/0263-7855(96)00018-5.
(19) Phillips, J. C.; Braun, R.; Wang, W.; Gumbart, J.; Tajkhorshid, E.; Villa, E.; Chipot, C.; Skeel, R. D.; Kalé, L.; Schulten, K. Scalable Molecular Dynamics with NAMD. *J Comput Chem* **2005**, *26* (16), 1781–1802. https://doi.org/10.1002/jcc.20289.
(20) Denning, E. J.; Priyakumar, U. D.; Nilsson, L.; Mackerell, A. D., Jr. Impact of 2'-Hydroxyl Sampling on the Conformational Properties of RNA: Update of the CHARMM All-Atom Additive Force Field for RNA. *J Comput Chem* **2011**, *32* (9), 1929–1943. https://doi.org/10.1002/jcc.21777.
(21) Hart, K.; Foloppe, N.; Baker, C. M.; Denning, E. J.; Nilsson, L.; MacKerell, A. D. Optimization of the CHARMM Additive Force Field for DNA: Improved Treatment of the Bi/Bii Conformational Equilibrium. *Journal of Chemical Theory and Computation* **2012**, *8* (1), 348–362. https://doi.org/10.1021/ct200723y.
(22) Darden, T.; York, D.; Pedersen, L. Particle Mesh Ewald: An Nlog(N) Method for Ewald Sums in Large Systems. *Journal of Chemical Physics* **1993**, *98* (12), 10089–10092. https://doi.org/10.1063/1.464397.
(23) Beyene, A. G.; Alizadehmojarad, A. A.; Dorlhiac, G.; Goh, N.; Streets, A. M.; Král, P.; Vuković, L.; Landry, M. P. Ultralarge Modulation of Fluorescence by Neuromodulators in Carbon Nanotubes Functionalized with Self-Assembled Oligonucleotide Rings. *Nano Letters* **2018**, *18* (11), 6995–7003. https://doi.org/10.1021/acs.nanolett.8b02937.
(24) Alizadehmojarad, A. A.; Zhou, X.; Beyene, A. G.; Chacon, K. E.; Sung, Y.; Pinals, R. L.; Landry, M. P.; Vuković, L. Binding Affinity and Conformational Preferences Influence Kinetic Stability of Short Oligonucleotides on Carbon Nanotubes. *Advanced Materials Interfaces* **2020**, *7* (15), 2000353. https://doi.org/10.1002/admi.202000353.
(25) Zheng, Y.; Alizadehmojarad, A. A.; Bachilo, S. M.; Kolomeisky, A. B.; Weisman, R. B. Dye Quenching of Carbon Nanotube Fluorescence Reveals Structure-Selective Coating Coverage. *ACS Nano* **2020**, *14* (9), 12148–12158. https://doi.org/10.1021/acsnano.0c05720.
(26) Shankar, A.; Mittal, J.; Jagota, A. Binding between DNA and Carbon Nanotubes Strongly Depends upon Sequence and Chirality. *Langmuir* **2014**, *30* (11), 3176–3183. https://doi.org/10.1021/la500013c.
(27) Jena, P. V.; Safaee, M. M.; Heller, D. A.; Roxbury, D. DNA-Carbon Nanotube Complexation Affinity and Photoluminescence Modulation Are Independent. *ACS Applied*

Materials and Interfaces **2017**, *9* (25), 21397–21405. https://doi.org/10.1021/acsami.7b05678.
(28) Zheng, Y.; Bachilo, S. M.; Weisman, R. B. Enantiomers of Single-Wall Carbon Nanotubes Show Distinct Coating Displacement Kinetics. *Journal of Physical Chemistry Letters* **2018**, *9* (13), 3793–3797. https://doi.org/10.1021/acs.jpclett.8b01683.
(29) Rocha, J. D.; Bachilo, S. M.; Ghosh, S.; Arepalli, S.; Weisman, R. B. Efficient Spectrofluorimetric Analysis of Single-Walled Carbon Nanotube Samples. *Analytical chemistry* **2011**, *83* (19), 7431–7437.
(30) Johnson, R. R.; Kohlmeyer, A.; Johnson, A. T. C.; Klein, M. L. Free Energy Landscape of a DNA - Carbon Nanotube Hybrid Using Replica Exchange Molecular Dynamics. *Nano Letters* **2009**, *9* (2), 537–541. https://doi.org/10.1021/n1802645d.